

Alleviating the Effect of Data Imbalance on Adversarial Training

Guanlin Li

Nanyang Technological University, S-Lab

guanlin001@e.ntu.edu.sg

Guowen Xu

City University of Hong Kong

guowenxu@cityu.edu.hk

Tianwei Zhang

Nanyang Technological University

tianwei.zhang@ntu.edu.sg

Abstract

*In this paper, we study adversarial training on datasets that obey the long-tailed distribution, which is practical but rarely explored in previous works. Compared with conventional adversarial training on balanced datasets, this process falls into the dilemma of generating uneven adversarial examples (AEs) and an unbalanced feature embedding space, causing the resulting model to exhibit low robustness and accuracy on tail data. To combat that, we theoretically analyze the lower bound of the robust risk to train a model on a long-tailed dataset to obtain the key challenges in addressing the aforementioned dilemmas. Based on it, we propose a new adversarial training framework – *Re-balancing Adversarial Training* (REAT). This framework consists of two components: (1) a new training strategy inspired by the effective number to guide the model to generate more balanced and informative AEs; (2) a carefully constructed penalty function to force a satisfactory feature space. Evaluation results on different datasets and model structures prove that REAT can effectively enhance the model’s robustness and preserve the model’s clean accuracy. The code can be found in <https://github.com/GuanlinLee/REAT>.*

1. Introduction

Adversarial attacks [7, 21] have become a serious threat to deep learning models, where the adversary crafts adversarial examples (AEs) by adding imperceptible perturbations to a clean input, to deceive the model into making wrong predictions. To mitigate adversarial attacks, a prominent way is adversarial training [21], which generates AEs and incorporates them into the training set to improve the model’s adversarial robustness.

However, existing efforts of adversarial training mainly focus on balanced datasets, while ignoring more realistic datasets obeying long-tailed distributions [3, 6, 19]. Informally, training data subject to a long-tailed distribution has the property that the vast majority of the data belong to a

minority of total classes (i.e., “head” classes), while the remaining data belong to other classes (“body” and “tail” classes) [29]. This distinct nature yields new problems in adversarial training (see Section 2.2 for detailed explanations). First, it is difficult to produce uniform and balanced adversarial examples (AEs): AEs are mainly misclassified by the model into the head classes with overwhelming probabilities regardless of the labels of their corresponding clean samples. Second, the excessive dominance of head classes in the feature embedding space further compresses the feature space of tail classes. The mutual entanglement of the above two problems leads to the underfitting of tail classes in both adversarial robustness and clean accuracy, thus leading to unsatisfactory training performance.

To address these challenges, [31] proposed RoBal, the first work (and the only work, to our best knowledge) towards adversarial training on datasets with long-tailed distributions. It is essentially a two-stage re-balancing adversarial training method. The first stage lies in the training process, where a new class-aware margin loss function is designed to make the model pay equal attention to data from head classes and tail classes. The second stage focuses on the inference process, where a pre-defined bias is added to the predicted logits vectors, thereby improving the prediction accuracy of samples from the tail classes. Moreover, RoBal constructs a new normalized cosine classification layer, to further improve models’ accuracy and adversarial robustness.

While RoBal shows impressive results on a variety of datasets, it still has several limitations. First, the robustness of RoBal benefits mainly from gradient obfuscation (specifically, gradient vanishing) [1] in the proposed new scale-invariant classification layer. This can be easily compromised by simply multiplying the logits by a constant, as the constant can increase the absolute value of gradients against gradient vanishing and correct the sign of gradients during AE generation (see Tables 3 and 4). Second, the designed class-aware margin loss ignores samples from body

arXiv:2307.10205v2 [cs.LG] 4 Dec 2023

classes and exclusively focuses on head and tail classes, which inevitably reduces the overall model accuracy. Details can be found in Sections 2.2 and 5.2.

To advance the practicality of adversarial training on long-tailed datasets, we design a new framework: Re-balancing adversarial training (REAT), which demonstrates higher clean accuracy and adversarial robustness compared to RoBal. Our insights come from the revisit of two key components in adversarial training: AE generation and feature embedding. Particularly, **for AE generation**, we force the generated AEs to be misclassified into each class as uniformly as possible, so that the information of the tail classes is sufficiently learned during adversarial training to improve the robustness. Our implementation is inspired by the effective number [6] in long-tailed recognition, which was proposed to increase the marginal benefits from data of tail classes. We generalize its definition to the AE generation process and propose a new Re-Balanced Loss (*RBL*) function. *RBL* dynamically adjusts the weights assigned to each class, which significantly improves the effectiveness of the original balanced loss. **For feature embedding**, it is challenging to balance the volume of each class’s feature space, especially if the size of each class varies. To address this issue, we propose a Tail-sample-mining-based feature margin regularization (*TAIL*) approach. *TAIL* treats the samples from tail classes as hard samples and optimizes feature embedding distributions of tail classes and others. To better fit the unbalanced data distribution, we propose a *joint weight* to increase the contribution of tail features in the entire feature embedding space. Visualization results can be found in the supplementary materials. We conduct comprehensive experiments on CIFAR-10-LT, CIFAR-100-LT, and Tiny-Imagenet datasets to demonstrate the superiority of REAT over existing methods. For instance, REAT achieves 67.33% clean accuracy and 32.08% robust accuracy under AutoAttack, which are 1.25% and 0.94% higher than RoBal.

We want to emphasize that REAT is not a simple combination of previous works. First, our method is based on the theoretical analysis. Furthermore, its superiority lies in the newly proposed modifications over previous methods, to adapt to the long-tailed adversarial training scenario. We validate that simply integrating existing methods cannot achieve satisfactory results. For instance, without generalizing the definition of effective number from normal training to AE generation, the original term will result in much lower performance (“ENR” in Table 2).

2. Background and Motivation

2.1. Long-tailed Recognition

Data in the wild usually obey a long-tailed distribution [3, 6, 19], where most samples belong to a small part of classes. Models trained on long-tailed datasets usually give higher confidence to the samples from head classes, which harms

the generalizability for the samples from the body or tail classes. It is challenging to solve such overconfidence issues under the long-tailed scenarios [2, 9, 14]. Several approaches have been proposed to achieve long-tailed recognition. For instance, (1) the re-sampling methods [8, 20, 24] generate balanced data distributions by sampling data with different frequencies in the training set. (2) The cost-sensitive learning methods [6, 11, 19] modify the training loss with additional weights to balance the gradients from each class. (3) The training phase decoupling methods [15, 16] first train a feature extractor on re-sampled balanced data, and then train a classifier on the original dataset. (4) The classifier designing methods [15, 31] modify the classification layer with prior knowledge to better fit the unbalanced data. More details about related works are in the supplementary materials.

2.2. Long-tailed Adversarial Training

Adversarial training is a promising solution to enhance the model’s robustness against AEs. Previous works mainly consider the balanced datasets. Discussions of these works can be found in the supplementary materials. When the training data become unbalanced, training a robust model becomes more challenging. As mentioned in Section 2.1, in long-tailed recognition, most data come from the head classes while the data of the tail classes are relatively scarce. This causes two consequences: unbalance in the output probability space and unbalance in the feature embedding space, which are detailed as follows.

First, we need to generate AEs on-the-fly during adversarial training. The unbalanced output probability space caused by long-tailed datasets can lead to unbalanced AEs, which cause the produced model to show unbalanced robustness across different classes. Figure 1 shows such an example. We adopt PGD-based adversarial training to train a ResNet-18 model and measure the distribution of the model’s predictions for the generated AEs during the training process. Figure 1a shows the case of a balanced training set (CIFAR-10). We observe that the predictions of the AEs are **uniformly distributed** among all the classes. In contrast, Figure 1b shows the case of an unbalanced training set (CIFAR-10-LT). Due to the long-tailed distribution, **most AEs are labeled as head classes**. This indicates that the final model has lower accuracy and robustness for tail classes, making it more vulnerable to adversarial attacks [5].

Second, in an unbalanced training set, the head classes can dominate the feature embedding space of the model, which can reduce the area of tail features. As a result, the performance and generalizability of the model for tail classes will be decreased. In contrast, a model trained on balanced data will give an even feature space for each class. Figure 2 compares the feature maps of AEs in these two scenarios, where we train ResNet-18 models with PGD-based adversar-

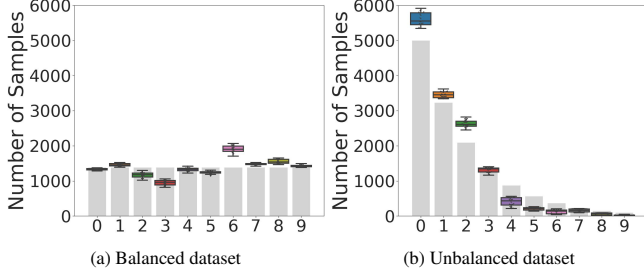


Figure 1. Prediction distributions of AEs. Clean label distributions are shown by gray bars.

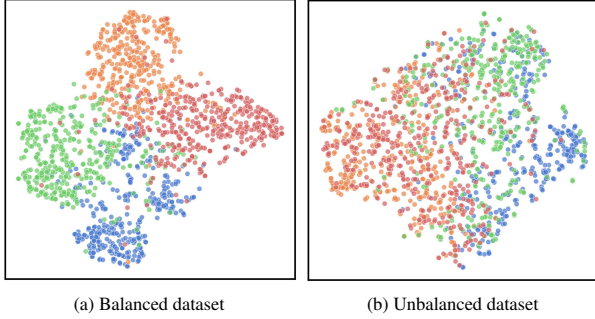


Figure 2. Visualization of feature maps of AEs from models.

ial training on balanced and unbalanced CIFAR-10¹. **The long-tailed scenario has larger differences between head and tail features compared to the balanced scenario.**

A straightforward way is to directly adopt existing solutions introduced in Section 2.1 (e.g., [3, 6, 19, 24]) for adversarial training, which can produce more balanced AE prediction distributions and feature embedding space. However, they can only partially address the overconfidence and underconfidence issues in model prediction, due to the lack of tail samples and AEs predicted as tail classes (see Section 5.2 and the supplementary materials). RoBal [31] is the first methodology dedicated to adversarial training with long-tailed datasets. It introduces a new loss function to promote the model to learn features from head classes and tail classes equally. It further replaces the traditional classification layer with a cosine classifier, where both weights and features are normalized and the outputs are multiplied by a temperature factor. In the inference phase, RoBal adjusts the output logits with a prior distribution, which is aligned with the label distribution. However, in our experiments, we find RoBal ignores the features from the body classes, which can harm the clean accuracy and robustness. Furthermore, RoBal can be easily defeated by a simple **adaptive attack**, which multiplies the output logits by a factor when generating AEs (see Section 5.2). This motivates us to explore a better solution for long-tailed adversarial training.

¹For better readability, we only show four classes (two head classes “airplane” (blue) and “automobile” (orange), and two tail classes “ship” (green) and “truck” (red)). The complete feature maps for 10 classes can be found in the supplementary materials.

3. Theoretical Analysis

Besides providing empirical studies in Section 2.2, we provide theoretical analysis to give a lower bound for robust risk, aiming to support the most vulnerable parts in models trained on a long-tailed dataset found in Section 2.2. To theoretically study the difficulties of adversarially training a model on unbalanced datasets, we first consider the robust risk $\mathcal{R}_{\text{rob}}(\theta)$, where θ stands for the parameters of a function f , which can be a deep learning model. Let $\mathcal{X}_i \subset \mathbb{R}^d$ be the input space for class i , and $\mathcal{Y} = \{1, \dots, C\}$ be the class set.

We consider a following dataset $\mathcal{D} = \{(x, i) | x \in \mathcal{X}_i, i \in \mathcal{Y}\}$, that for class i , we only have n_i data in it. Then, we define that $p_\theta(\cdot | x) = \text{softmax}(f_\theta(x)) \in \mathbb{R}^C$ and $F_\theta(x) = \text{argmax}[f_\theta(x)] \in \mathcal{Y}$. Given a perturbed set $\mathcal{B}_p(x_i, \epsilon) = \{x'_i \in \mathcal{X}_i | \|x_i - x'_i\|_p \leq \epsilon\}$, we have $\mathcal{R}_{\text{rob}}(\theta) = \mathbb{E}_{\mathcal{D}}[\max_{x'_i \in \mathcal{B}_p(x_i, \epsilon)} \mathbb{1}\{F_\theta(x'_i) \neq i\}]$.

Assume that for each class i , its $p_\theta(\cdot | x_i)$ is independent to other class $j \neq i$. We have $\mathcal{R}_{\text{rob}}(\theta) = \sum_{i=1}^C \frac{1}{n_i} \sum_{j=1}^{n_i} \max_{x' \in \mathcal{B}_p(x_i^j, \epsilon)} \mathbb{1}\{F_\theta(x') \neq i\} p(i)$. Let $\mathcal{R}_{\text{rob}}^i(\theta) = \sum_{j=1}^{n_i} \max_{x' \in \mathcal{B}_p(x_i^j, \epsilon)} \mathbb{1}\{F_\theta(x') \neq i\} p(i)$, which can be further decomposed of two terms, i.e., the natural risk and the boundary risk [35], i.e.,

$$\begin{aligned} \mathcal{R}_{\text{rob}}^i(\theta) &= \mathcal{R}_{\text{nat}}^i(\theta) + \mathcal{R}_{\text{bdy}}^i(\theta) = \sum_{j=1}^{n_i} \mathbb{1}\{F_\theta(x_i^j) \neq i\} p(i) \\ &\quad + \sum_{j=1}^{n_i} \mathbb{1}\{\exists x' \in \mathcal{B}_p(x_i^j, \epsilon), F_\theta(x') \neq i\} p(i). \end{aligned}$$

We notice that for an unbalanced dataset, $p(i) = \frac{n_i}{\sum_{i=1}^C n_i}$. Therefore, we have the following lower bound for the robust risk $\mathcal{R}_{\text{rob}}(\theta)$.

Theorem 1 *Given a function f_θ and dataset \mathcal{D} , which we defined above, let*

$$g(x) \in \text{argmax}_{x' \in \mathcal{B}_p(x, \epsilon)} \mathbb{1}\{F_\theta(x) \neq F_\theta(x')\}$$

Assume that a larger n_i will decrease the $\mathcal{R}_{\text{rob}}^i(\theta)$, and vice versa. Then, we have

$$\begin{aligned} \mathcal{R}_{\text{rob}}(\theta) &\geq \sum_{i=1}^C \frac{1}{C} \left(\sum_{j=1}^{n_i} \mathbb{1}\{F_\theta(x_i^j) \neq i\} \right. \\ &\quad \left. + \sum_{j=1}^{n_i} \mathbb{1}\{F_\theta(g(x_i^j)) \neq F_\theta(x_i^j)\} \right) \end{aligned}$$

The proof can be found in the supplementary materials. In Theorem 1, $\mathbb{1}\{F_\theta(x_i^j) \neq i\}$ is the error for clean data x_i^j , and $\mathbb{1}\{F_\theta(g(x_i^j)) \neq F_\theta(x_i^j)\}$ is a general robust error, which means that the prediction of the perturbed data disagrees with the prediction of the clean data. Specifically, $\mathbb{1}\{F_\theta(x_i^j) \neq i\}$ reflects the **representation entangling** to some degree. And $g(x)$ can represent the **predicted label distribution of**

adversarial examples. These two terms are aligned with the findings in Section 2.2. Therefore, the theoretical analysis supports the motivation of balancing the label distribution of adversarial examples and aligning feature representations.

4. Methodology

We introduce REAT, a new framework for adversarial training on unbalanced datasets. REAT includes two innovations to address the two issues disclosed in Section 2.2 and 3. Specifically, to balance the AE distribution and encourage the model to learn more information from tail samples, we modify the objective function in the AE generation process with weights calculated based on the effective number [6]. To balance the feature embedding space, we propose a loss term to increase the area of features from tail classes.

Preliminaries. We first give formal definitions of a long-tailed dataset. Consider a dataset containing C classes with N_i samples in each class i . We assume the classes are sorted in the descending order based on the number of samples in each class, i.e., $N_i \geq N_{i+1}$. The unbalanced ratio is defined as $UR = \frac{N_1}{N_C}$ [3]. Following previous works [6, 29], a long-tailed dataset can be divided into three parts: (1) i is a head class (HC) if $1 \leq i \leq \lfloor \frac{C}{3} \rfloor$, where $\lfloor x \rfloor$ is a floor function; (2) i is a tail class (TC) if $\lceil \frac{2C}{3} \rceil \leq i \leq C$, where $\lceil x \rceil$ is a ceiling function; (3) The rest are body classes (BC). Below, we describe the detailed mechanisms of REAT.

4.1. Re-balancing AEs

For adversarial training, it is desirable that the objective function could encourage AEs that are classified into rarely-seen classes while punishing AEs that are classified into abundant classes. To realize this in the long-tailed scenario, we borrow the idea of the effective number from [6] and generalize it to adversarial training. The effective number is mainly used to measure the data overlap of each class. For class i containing N_i data, its effective number is defined as $E_{N_i} = \frac{1-\beta^{N_i}}{1-\beta}$, where $\beta = \frac{\sum N_i - 1}{\sum N_i}$. Given the effective numbers E_{N_i} and E_{N_j} , if $E_{N_i} > E_{N_j}$, the marginal benefit obtained from increasing the number of training samples in class i is less than increasing the same number of training samples in class j [6]. This implies that we can adopt the effective number as a guide to balance the distribution of AEs generated during training.

Motivation. We explain the motivation of using the effective number in AE generation as follows. At a high level, *the generation of AEs can be viewed as a data sampling process*, i.e., AEs are essentially sampled from the neighbors of their corresponding clean samples. Therefore, we can calculate the effective number between AEs generated in two consecutive epochs, and use it as the basis to assign dynamic weights to each class in the loss function, inducing the model to produce as many less overlapped AEs as pos-

sible in consecutive epochs. This implicitly generates more AEs that are classified into tail classes and makes the model extract more marginal benefits from samples of tail classes, thus achieving our purpose.

Technical design. For simplicity, we assume that the predicted label distributions (i.e., labels assigned by the model M for AEs) in two successive training epochs will stay stable and not change too much, **which has been proven in [36]**. Then, in epoch $k - 1$, we count the number of AEs that are classified into each class, denoted as $\mathbf{n} = [n_1, n_2, \dots, n_C]$.² As a result, generating AEs in epoch k can be approximated as sampling new AEs after sampling n_i data for each class i . Therefore, we can compute the effective number of class i as $E_{n_i} = \frac{1-\beta_i^{n_i}}{1-\beta_i}$, where $\beta_i = \frac{N_i-1}{N_i}$. Note that our β is *class-related* to assign finer convergence parameters for each class, which is different from the calculation in [6]. We will experimentally prove that this adaptive effective number can better improve the model robustness in Section 5.1.

Based on the property that the effective number of each class is inversely proportional to the marginal benefit of the new samples of this class, we construct a new indicator variable weight w_i for the marginal benefit, which is inversely proportional to E_{n_i} . This weight can be used to correct the loss in the AE generation process. Specifically, following the class-balanced softmax cross-entropy loss proposed in [6], we compute the weight w_i for class i as follows:

$$w_i = \frac{C}{E_{n_i} \sum_{j=1}^C \frac{1}{E_{n_j}}} \quad (1)$$

With the weight w_i for each class i , we design a new Re-Balancing Loss (RBL) function as below:

$$RBL = -w_i * \log \frac{e^{z_i}}{\sum_j e^{z_j}} \quad (2)$$

where $\log \frac{e^{z_i}}{\sum_j e^{z_j}}$ is the original loss function adopted to generate AEs. Our goal is to maximize RBL to generate AEs for adversarial training.

Analysis. We analyze why RBL can help generate balanced AEs from unbalanced data samples. First, we show the effective number enjoys the *asymptotic properties*: (1) when $n_i \rightarrow 0$, we have $E_{n_i} \rightarrow 0$ and $w_i \rightarrow C$; (2) when $n_i \rightarrow \infty$, we have $E_{n_i} \rightarrow \frac{1}{1-\beta_i}$ and $w_i \rightarrow 0$, as there exists $E_{n_j} \rightarrow 0, i \neq j$. Based on the asymptotic properties, if there are many AEs assigned to the label of class i in epoch $k - 1$, then in epoch k , the increased effective number E_{n_i} results in a smaller w_i . As a consequence, RBL will induce AEs generated in this round with minimized data overlap compared to AEs of the previous round, which implicitly generates more AEs that are classified into other classes. Our experiments in Section 5.2 indicate that combined with long-tailed recognition losses, RBL can better balance the AE

²For the first training epoch, we directly use the number of clean data N_i in each class as the prior distribution.

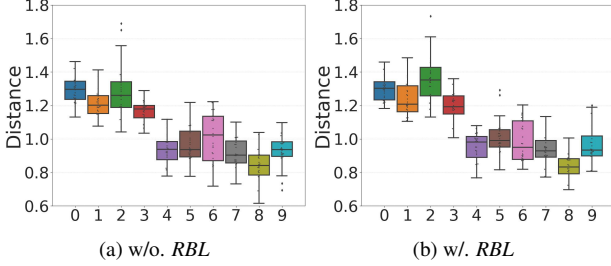


Figure 3. Distributions of Euclidean distances of AEs generated from the same clean data in consecutive training epochs.

generation process and increase the number of AEs predicted into tail classes by $5\times$. Figure 3 compares the distances of AEs between two consecutive training epochs without and with *RBL*. The models (ResNet-18) are trained on CIFAR-10-LT with the unbalanced ratio $UR=50$. A smaller distance indicates a larger overlap of the two AEs and less marginal benefit the model can obtain from the process. We observe that *RBL* is able to increase the distances of AEs from tail classes, and generate more informative AEs to enhance the model’s robustness.

4.2. Tail Feature Alignment

From Figure 2, we find the feature space of tail classes is smaller than that of head classes, making the model lean to classify the input into head classes. So, it is important to expand the feature space for tail classes to balance the feature representation. To achieve this goal, we first define a probabilistic feature embedding space as $\mathbf{f}^p = [\frac{e^{f_1}}{\sum_j e^{f_j}}, \frac{e^{f_2}}{\sum_j e^{f_j}}, \dots, \frac{e^{f_K}}{\sum_j e^{f_j}}] = [f_1^p, f_2^p, \dots, f_K^p]$, where f_i is the i -th feature before the final classification layer, and K is the feature dimension. The motivation of using a probabilistic feature embedding space is to overcome the scale changes in feature representations caused by the unbalanced data distribution [31]. For each class i , we assume the probabilistic feature is sampled from a distribution \mathcal{D}_i^f . As a result, given any two classes $i \in TC$ and $j \in HC \cup BC$, our goal is to maximize the difference between \mathcal{D}_i^f and \mathcal{D}_j^f , thereby rebalancing the distributions of different classes in the feature space and making them more divisible.

We design a Tail-sample-mining-based feature margin regularization (*TAIL*) approach to achieve this goal. Algorithm 1 describes its detailed mechanism. Specifically, let $\mathbf{F}^p = [\mathbf{f}_1^p, \mathbf{f}_2^p, \dots, \mathbf{f}_B^p]$ denote all probabilistic features of a batch containing B samples, and $\mathbf{y} = [y_1, y_2, \dots, y_B]$ denote the labels of the corresponding feature representations. The class weights $\Omega = [\omega_1, \omega_2, \dots, \omega_C]$ are calculated based on the smoothed inverse class frequency [22, 23], i.e., $\omega_i = \sqrt{\frac{\sum_j N_j}{N_i}}$, implying tail classes have larger class weights than head classes. The core component of *TAIL* is the computation of the regularization term R , which is

Algorithm 1 *TAIL*

```

1: Input: probabilistic feature batch  $\mathbf{F}^p$ , label  $\mathbf{y}$ ,
   class weights  $\Omega$ , tail classes  $TC$ , batch size  $B$ 
2:  $R \leftarrow 0, S \leftarrow 0$ 
3: for  $i = 1 \rightarrow B$  do
4:   if  $y_i \in TC$  then
5:      $S = S + 1$ 
6:     Update  $R$  following Equation 3
7:   end if
8: end for
9: if  $S = 0$  then
10:  return 0
11: else
12:  return  $\frac{R}{S}$ 
13: end if

```

updated for each $y_i \in TC$ using the following equation:

$$R = R - \frac{1}{B} \sum_{j=1}^B (-1)^{\mathbb{1}(y_i=y_j)} (\omega_i + \omega_j) \sum_{k=1}^K f_{j,k}^p \log \frac{f_{j,k}^p}{f_{i,k}^p} \quad (3)$$

where $\mathbb{1}(y_i = y_j)$ is the indicator function (outputting 1 if $y_i = y_j$, and 0 otherwise), and the initial value of R is 0. In Equation 3, we first compute the feature distribution differences using the Kullback–Leibler divergence (KLD): $\sum_{k=1}^K f_{j,k}^p \log \frac{f_{j,k}^p}{f_{i,k}^p}$, where $f_{i,k}^p$ is the value of the k -th dimension in the probabilistic feature \mathbf{f}_i^p for the i -th sample. A larger KLD value means a larger difference between the distributions of the feature embeddings of the i -th and j -th samples. Hence, with the property of R , for each batch, we can maximize the distributional differences between $\mathcal{D}_i^f, i \in TC$ and $\mathcal{D}_j^f, j \neq i, j \in [C]$, and minimize the distributional gap for samples from the same tail class. To further enhance the influence of the regularization term among tail classes, we assign a *joint weight* $(\omega_i + \omega_j)$ to the feature pair $(\mathbf{f}_i^p, \mathbf{f}_j^p)$. ω_i for tail samples is bigger than that for head samples. To increase the distinction between pairs of tail classes and non-tail classes and pairs of two tail classes, the joint weight further strengthens the effect of the regularization for pairs of two tail classes, thus improving the performance. Finally, we adopt the average distance inside the batch: $\frac{R}{S}$.

Note that our regularization term *TAIL* is general and can be used with any other long-tailed recognition loss function L_{lt} in the following form:

$$L = L_{lt} + TAIL$$

To summarize, the training pipeline of our REAT uses *RBL* to generate adversarial examples, from which it trains the robust model with the loss function L .

5. Experiments

Datasets and Models. We evaluate REAT on CIFAR-10-LT and CIFAR-100-LT, which are the mainstream datasets

Losses	Method	Clean Accuracy	PGD-20	PGD-100	CW-100	AA
FL	PGD-AT	53.58(0.81)	30.88(0.24)	30.85(0.25)	28.48(0.59)	27.00(0.60)
	REAT	55.22 (1.42)	31.14 (0.34)	31.08 (0.33)	28.71 (0.53)	27.23 (0.56)
EN	PGD-AT	55.26 (0.38)	31.82(0.36)	31.75(0.40)	29.91(0.27)	28.26(0.22)
	REAT	55.25(0.87)	32.20 (0.25)	32.14 (0.23)	30.12 (0.33)	28.69 (0.48)
LDAM	PGD-AT	52.74(0.71)	31.31(0.25)	31.24(0.23)	29.41(0.42)	28.03(0.37)
	REAT	53.47 (1.04)	31.52 (0.27)	31.52 (0.27)	29.63 (0.25)	28.20 (0.21)
BSL	PGD-AT	66.99(0.17)	35.23(0.45)	35.01(0.43)	33.17(0.37)	31.15(0.49)
	REAT	67.33 (0.45)	36.20 (0.06)	36.02 (0.09)	33.98 (0.23)	32.08 (0.12)

Table 1. Results on CIFAR-10-LT (UR=50) with different long-tailed recognition losses. For this and the following tables, standard errors are shown inside (). Best results are in bold.

Rebalancing	Method	Clean Accuracy	PGD-20	PGD-100	CW-100	AA
-		66.99(0.17)	35.23(0.45)	35.01(0.43)	33.17(0.37)	31.15(0.49)
RW	PGD-AT	66.82(0.40)	35.80(0.05)	35.65(0.08)	33.29(0.32)	31.40(0.31)
RWS		67.28(0.63)	35.83(0.35)	35.70(0.37)	33.38(0.50)	31.50(0.67)
ENR		66.53(0.91)	35.26(0.14)	35.08(0.12)	32.95(0.27)	31.05(0.13)
BRW		67.98 (0.09)	34.65(0.30)	34.47(0.32)	33.55(0.33)	31.36(0.40)
<i>RBL</i>		w/o <i>TAIL</i>	67.46(0.65)	35.59(0.18)	35.48(0.19)	33.51(0.39)
<i>RBL</i>	w <i>TAIL</i>	67.33(0.45)	36.20 (0.06)	36.02 (0.09)	33.98 (0.23)	32.08 (0.12)

Table 2. Comparisons between different AE generation re-balancing strategies. *BSL loss is adopted.*

for evaluating long-tailed recognition tasks [3, 6, 24, 31]. Furthermore, we evaluate our method on a large dataset from the real world, Tiny-Imagenet [18], in the supplementary materials. To generate the unbalanced dataset, we follow the approach in [3] to set the unbalanced ratio (UR) as {10, 20, 50, 100} for CIFAR-10-LT and {10, 20, 50} for CIFAR-100-LT. We choose ResNet-18 (ResNet) [10] and WideResNet-28-10 (WRN) [34] as the target models.

Baselines. We consider two baselines. The first one is to *simply combine existing adversarial training methods with various long-tailed recognition losses*. Our experiments and analysis in the supplementary materials show that some adversarial training methods cannot converge well with the long-tailed recognition loss, such as TRADES [35], AWP [31] and MART [28]. So we choose the most effective one: PGD-AT [21]. The second baseline is RoBal [31].

Implementation. In our experiments, the number of training epochs is 80. The learning rate is 0.1 at the beginning and decayed in epochs 60 and 75 with a factor of 0.1. The weight decay is 0.0005. We adopt SGD to optimize the model parameters with a batch size of 128. We save the model with the highest robustness on the test set. For adversarial training, we adopt l_∞ -norm PGD [21], with a maximum perturbation size $\epsilon = 8/255$ for 10 iterations, and step length $\alpha = 2/255$ in each iteration. For each configuration, we report the mean and standard error under three repetitive experiments with different random seeds. Training with REAT is efficient and does not incur significant costs, as demonstrated in the supplementary materials.

Attacks. We mainly consider the l_∞ -norm attacks to evaluate the model’s robustness. The results under the l_2 -norm

attacks can be found in the supplementary materials. We choose four representative attacks: PGD attack [21] with the cross-entropy loss under 20 and 100 steps (PGD-20 and PGD-100), PGD attack with the C&W loss [4] under 100 steps (CW-100), and AutoAttack [5] (AA).

5.1. Ablation Studies

Impact of Long-tailed Recognition Losses. REAT is general and can be combined with different long-tailed recognition losses. We select four state-of-the-art losses and add each one with *TAIL* to evaluate REAT: focal loss (FL) [19], effective number loss (EN) [6], label-distribution-aware margin loss (LDAM) [3], and balanced softmax loss (BSL) [24]. For comparisons, we also choose PDG-AT and replace the original cross-entropy loss with the above long-tailed recognition loss for model parameter optimization.

Table 1 shows the comparison results with ResNet-18 and CIFAR-10-LT (UR=50). We obtain two observations. (1) BSL loss can significantly outperform other long-tailed recognition losses for clean accuracy as well as adversarial robust accuracy against different attacks. So in the rest of our paper, *we mainly adopt this choice for evaluations*. (2) REAT achieves better adversarial robustness than PGD-AT for whatever loss function is adopted to train the model. Furthermore, the clean accuracy is improved in most cases when REAT is used. Therefore, we conclude that REAT has strong generalization and applicability to different recognition losses.

Impact of AE Generation Re-balancing Losses. We then compare the effectiveness of our *RBL* with various rebalancing methods adopted in the AE generation process. We

UR	Method	Clean Accuracy	PGD-20	PGD-100	CW-100	AA
10	RoBal	75.33(0.39)	45.98(0.39) Adaptive: 41.25	45.97(0.39) Adaptive: 41.13	41.02(0.02)	39.30(0.10)
	REAT	75.20(0.03)	42.97(0.17)	42.76(0.19)	41.52(0.22)	39.25(0.21)
20	RoBal	71.92(0.62)	43.23(0.25) Adaptive: 38.45	43.19(0.22) Adaptive: 38.20	38.23(0.07)	36.17(0.28)
	REAT	72.73(0.50)	40.57(0.15)	40.41(0.12)	38.55(0.29)	36.53(0.21)
50	RoBal	66.08(0.69)	38.46(0.18) Adaptive: 33.54	38.44(0.11) Adaptive: 33.20	33.90(1.72)	31.14(0.44)
	REAT	67.33(0.45)	36.20(0.06)	36.02(0.09)	33.98(0.23)	32.08(0.12)
100	RoBal	60.11(0.62)	36.08(0.18) Adaptive: 30.55	36.05(0.20) Adaptive: 30.36	30.57(0.77)	28.64(0.28)
	REAT	63.92(0.68)	32.84(0.07)	32.69(0.15)	30.73(0.38)	28.90(0.33)

Table 3. Results on CIFAR-10-LT with different values of UR. Red numbers represent the results under our adaptive attack.

UR	Method	Clean Accuracy	PGD-20	PGD-100	CW-100	AA
10	RoBal	43.47(0.31)	20.55(0.20) Adaptive: 18.49	20.49(0.20) Adaptive: 18.31	18.12(0.23)	16.86(0.10)
	REAT	45.94(0.15)	19.26(0.18)	19.16(0.18)	17.99(0.09)	16.58(0.06)
20	RoBal	39.58(0.40)	17.73(0.11) Adaptive: 16.00	17.71(0.08) Adaptive: 15.93	15.58(0.11)	14.55(0.10)
	REAT	41.98(0.21)	16.84(0.10)	16.72(0.12)	15.77(0.23)	14.45(0.20)
50	RoBal	34.24(0.54)	14.77(0.09) Adaptive: 13.22	14.77(0.10) Adaptive: 13.18	12.77(0.10)	12.02(0.08)
	REAT	37.43(0.37)	14.25(0.22)	14.18(0.26)	13.38(0.15)	12.32(0.17)

Table 4. Results on CIFAR-100-LT with different URs. Red numbers represent the results under our adaptive attack.

replace the cross-entropy with four SOTA rebalancing strategies: (1) ReWeight (RW) [12, 29]; (2) ReWeight Smooth (RWS) [22, 23]; (3) Effective Number Reweight (ENR) [6]; (4) Balanced Softmax ReWeight (BRW) [24].

Table 2 shows the comparison results on CIFAR-10-LT (UR=50) with the ResNet-18 model structure. We observe that the considered strategies can indeed increase the clean accuracy and robustness of the final models by re-balancing the generated AEs. Particularly, our *RBL* outperforms other approaches, giving better robustness under different attacks. Furthermore, our dynamic effective number achieves better results than the original effective number implementation (ENR), in which the model adopts labels of the clean data to balance the AE generation. This is because our adaptive effective number allows the samples to equally learn features of both head and tail classes, and makes the model obtain more marginal benefit from the AEs. By combining *RBL* and *TAIL*, REAT achieves the best results under various attacks, which proves the effectiveness of the AE re-balancing and feature distribution alignment strategy.

5.2. Evaluation under Various Settings

To the best of our knowledge, RoBal [31] is the only work specifically focusing on adversarial training on unbalanced datasets. As analyzed in Section 2.2, there are several lim-

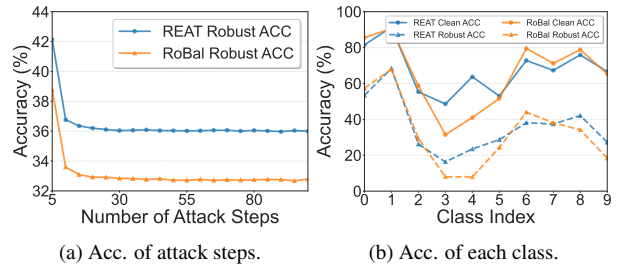


Figure 4. More comparisons results between REAT and RoBal for clean accuracy and adversarial robustness.

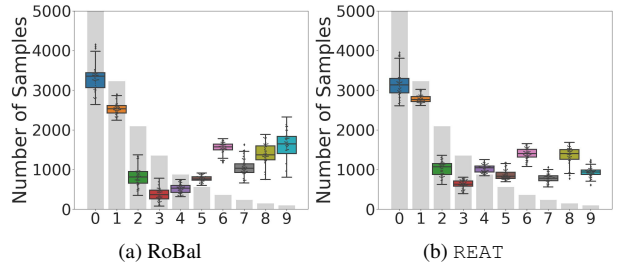


Figure 5. Distributions of model predictions for AEs during training. Clean label distributions are shown by gray bars.

itations in RoBal. Besides, we find that the scale-invariant classification layer in RoBal can **cause gradient vanishing** when generating AEs with the cross-entropy loss. It is because the normalized weights of the classification layer and

Method		Clean Accuracy	PGD-20	PGD-100	CW-100	AA
ResNet	RoBal	66.08(0.69)	38.46(0.18) Adaptive: 33.54	38.44(0.11) Adaptive: 33.20	33.90(1.72)	31.14(0.44)
	REAT	67.33 (0.45)	36.20 (0.06)	36.02 (0.09)	33.98 (0.23)	32.08 (0.12)
WRN	RoBal	69.33(0.11)	39.97(0.30) Adaptive: 34.58	39.98(0.32) Adaptive: 34.26	34.83(0.21)	33.09(0.41)
	REAT	72.58 (0.31)	36.53 (0.31)	36.35 (0.32)	35.30 (0.37)	33.37 (0.37)

Table 5. Results on CIFAR-10-LT (UR=50) with different model structures. Red numbers represent the results under our adaptive attack.

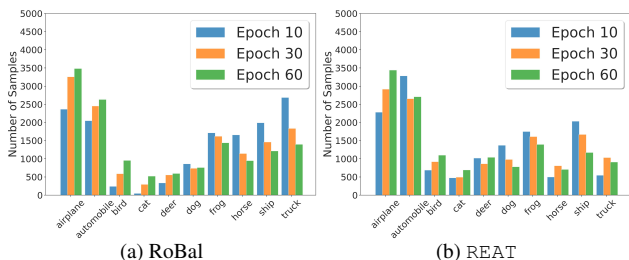


Figure 6. The distribution of model predictions for AEs in Epoch {10, 30, 60} on CIFAR-10-LT (UR=50).

the normalized features greatly reduce the scale of the gradients, making it fail to generate powerful AEs. We propose a simple adaptive attack to break the gradient vanishing and invalidate RoBal: the adversary can multiply the output logits by a factor (10 in all cases) when generating AEs, and then use these AEs to attack RoBal. This can significantly decrease the adversarial robustness of the trained model.

We perform experiments to compare RoBal and REAT from different perspectives, as shown in Tables 3 and 4. We adopt the CIFAR-10-LT and CIFAR-100-LT with ResNet-18 settings, respectively. In Table 5, we compare the results under different model structures on CIFAR-10. More results with different configurations can be found in the supplementary materials. First, for PGD-based attacks, we show that the model robustness partially originates from the gradient vanishing, and our adaptive attack can successfully break this effort. CW attack and AA can break the gradient obfuscation in the classification layer to some degree, due to the different loss functions in the AE generation process. Therefore, we do not design adaptive attacks for them. Second, comparing the results of RoBal and REAT under different values of UR, **REAT can achieve higher clean accuracy and robustness**, especially with larger UR. Third, for different model architectures, we prove that REAT outperforms RoBal consistently. This indicates REAT is a better training strategy for highly unbalanced datasets.

Furthermore, Figure 4a illustrates the robust accuracy of ResNet-18 on CIFAR-10-LT (UR=50) under different numbers of PGD attack steps. It proves that our REAT outperforms RoBal under all attack budgets. Figure 4b plots the accuracy of ResNet-18 on CIFAR-10-LT (UR=50) under the PGD-20 attack for each class. Our REAT can **achieve**

higher clean accuracy and robust accuracy on “body” classes, which will be explained below. More results can be found in the supplementary materials.

Interpretation. We perform an in-depth analysis of the comparisons between RoBal and REAT. We show the distributions of the predicted labels of AEs during adversarial training for these two approaches in Figure 5 and 6. We choose the configurations of CIFAR-10-LT (UR=50) and ResNet-18. Results under other configurations can be found in the supplementary materials. For RoBal, we observe that there are fewer AEs classified into body classes and more AEs classified into tail classes, indicating that **RoBal makes the model pay more attention to head and tail classes while overlooking the body classes**. In contrast, **REAT treats the body and tail classes more equally**, and this is one reason to achieve better performance on the “body” classes. Furthermore, we plot the feature embedding space with the t-SNE tool in the supplementary materials for feature-level comparison.

Summary. First, from the results, our solution brings more benefit than RoBal, as shown in Table 3. RoBal can sometimes hurt the robustness and clean accuracy. Second, we prove the robustness from RoBal partially depends on the gradient obfuscation and can be defeated by an adaptive attack. Third, through the results of PGD-AT with BSL loss, RoBal, and REAT, we find that compared with improving the robustness, it is easier to enhance the clean accuracy, which is consistent with the conclusion from [31]. To explore the reason behind this phenomenon, we analyze the difficulty and challenges of adversarial training on long-tailed datasets in the supplementary materials. All in all, improving robustness requires more data, and the number of data in the tail classes is not enough to train a model with high robustness, which is a big challenge in adversarial training. How to further improve it is our future work.

6. Conclusion

In this paper, we propose REAT, a new long-tailed adversarial training framework to improve the training performance on unbalanced datasets. Our method is inspired by our theoretical analysis of the lower bound of robust risk when training on a long-tailed dataset. Our analysis shows that the label distribution of adversarial examples and the feature representations can be key points in reducing robust risk.

Specifically, we present two novel components, *RBL* for promoting the model to generate balanced AEs, and a regularization term *TAIL* for forcing the model to assign larger feature spaces for tail classes. With these techniques, *REAT* helps models achieve state-of-the-art results and outperforms existing solutions on different datasets and model structures. There still exists a robustness gap between the ideal result obtained in the balanced setting and our approach. In the future, we aim to keep reducing this gap with more advanced solutions, e.g., new robust network structures or training loss functions.

References

- [1] Anish Athalye, Nicholas Carlini, and David A. Wagner. Obfuscated Gradients Give a False Sense of Security: Circumventing Defenses to Adversarial Examples. In *Proc. of the ICML*, pages 274–283, 2018. [1](#)
- [2] Mateusz Buda, Atsuto Maki, and Maciej A Mazurowski. A systematic study of the class imbalance problem in convolutional neural networks. *Neural networks*, 106:249–259, 2018. [2](#)
- [3] Kaidi Cao, Colin Wei, Adrien Gaidon, Nikos Aréchiga, and Tengyu Ma. Learning Imbalanced Datasets with Label-Distribution-Aware Margin Loss. In *Proc. of the NeurIPS*, pages 1565–1576, 2019. [1](#), [2](#), [3](#), [4](#), [6](#), [10](#)
- [4] Nicholas Carlini and David Wagner. Towards Evaluating the Robustness of Neural Networks. In *Proc. of the SP*, pages 39–57, 2017. [6](#)
- [5] Francesco Croce and Matthias Hein. Reliable evaluation of adversarial robustness with an ensemble of diverse parameter-free attacks. In *Proc. of the ICML*, pages 2206–2216, 2020. [2](#), [6](#)
- [6] Yin Cui, Menglin Jia, Tsung-Yi Lin, Yang Song, and Serge J. Belongie. Class-Balanced Loss Based on Effective Number of Samples. In *Proc. of the CVPR*, pages 9268–9277, 2019. [1](#), [2](#), [3](#), [4](#), [6](#), [7](#), [10](#)
- [7] Ian J. Goodfellow, Jonathon Shlens, and Christian Szegedy. Explaining and Harnessing Adversarial Examples. In *Proc. of the ICLR*, 2015. [1](#)
- [8] Hui Han, Wenyuan Wang, and Binghuan Mao. Borderline-SMOTE: A New Over-Sampling Method in Imbalanced Data Sets Learning. In *Proc. of the ICIC*, pages 878–887, 2005. [2](#), [10](#)
- [9] Haibo He and Eduardo A Garcia. Learning from imbalanced data. *IEEE Transactions on knowledge and data engineering*, 21(9):1263–1284, 2009. [2](#)
- [10] Kaiming He, Xiangyu Zhang, Shaoqing Ren, and Jian Sun. Deep Residual Learning for Image Recognition. In *Proc. of the CVPR*, pages 770–778, 2016. [6](#)
- [11] Youngkyu Hong, Seungju Han, Kwanghee Choi, Seokjun Seo, Beomsu Kim, and Buru Chang. Disentangling Label Distribution for Long-Tailed Visual Recognition. In *Proc. of the CVPR*, pages 6626–6636, 2021. [2](#), [10](#)
- [12] Chen Huang, Yining Li, Chen Change Loy, and Xiaoou Tang. Learning Deep Representation for Imbalanced Classification. In *Proc. of the CVPR*, pages 5375–5384, 2016. [7](#), [10](#)
- [13] Lang Huang, Chao Zhang, and Hongyang Zhang. Self-Adaptive Training: beyond Empirical Risk Minimization. In *Proc. of the NeurIPS*, 2020. [10](#)
- [14] Nathalie Japkowicz and Shaju Stephen. The class imbalance problem: A systematic study. *Intelligent data analysis*, 6(5): 429–449, 2002. [2](#)
- [15] Bingyi Kang, Saining Xie, Marcus Rohrbach, Zhicheng Yan, Albert Gordo, Jiashi Feng, and Yannis Kalantidis. Decoupling Representation and Classifier for Long-Tailed Recognition. In *Proc. of the ICLR*, 2020. [2](#), [10](#)
- [16] Bingyi Kang, Yu Li, Sa Xie, Zehuan Yuan, and Jiashi Feng. Exploring Balanced Feature Spaces for Representation Learning. In *Proc. of the ICLR*, 2021. [2](#), [10](#)
- [17] Salman H. Khan, Munawar Hayat, Syed Waqas Zamir, Jianbing Shen, and Ling Shao. Striking the Right Balance With Uncertainty. In *Proc. of the CVPR*, pages 103–112, 2019. [10](#)
- [18] Ya Le and Xuan Yang. Tiny imagenet visual recognition challenge. *CS 231N*, 7(7):3, 2015. [6](#)
- [19] Tsung-Yi Lin, Priya Goyal, Ross B. Girshick, Kaiming He, and Piotr Dollár. Focal Loss for Dense Object Detection. In *Proc. of the ICCV*, pages 2999–3007, 2017. [1](#), [2](#), [3](#), [6](#), [10](#)
- [20] Xu-Ying Liu, Jianxin Wu, and Zhi-Hua Zhou. Exploratory Undersampling for Class-Imbalance Learning. *IEEE Transactions on Systems, Man, and Cybernetics, Part B*, 39(2): 539–550, 2009. [2](#), [10](#)
- [21] Aleksander Madry, Aleksandar Makelov, Ludwig Schmidt, Dimitris Tsipras, and Adrian Vladu. Towards Deep Learning Models Resistant to Adversarial Attacks. In *Proc. of the ICLR*, 2018. [1](#), [6](#), [10](#)
- [22] Dhruv Mahajan, Ross B. Girshick, Vignesh Ramanathan, Kaiming He, Manohar Paluri, Yixuan Li, Ashwin Bharambe, and Laurens van der Maaten. Exploring the Limits of Weakly Supervised Pretraining. In *Proc. of the ECCV*, pages 185–201, 2018. [5](#), [7](#)
- [23] Tomáš Mikolov, Ilya Sutskever, Kai Chen, Gregory S. Corrado, and Jeffrey Dean. Distributed Representations of Words and Phrases and their Compositionality. In *Proc. of the NeurIPS*, pages 3111–3119, 2013. [5](#), [7](#)
- [24] Jiawei Ren, Cunjun Yu, Shunan Sheng, Xiao Ma, Haiyu Zhao, Shuai Yi, and Hongsheng Li. Balanced Meta-Softmax for Long-Tailed Visual Recognition. In *Proc. of the NeurIPS*, 2020. [2](#), [3](#), [6](#), [7](#), [10](#)
- [25] Leslie Rice, Eric Wong, and J. Zico Kolter. Overfitting in adversarially robust deep learning. In *Proc. of the ICML*, pages 8093–8104, 2020. [10](#)
- [26] Kaihua Tang, Jianqiang Huang, and Hanwang Zhang. Long-Tailed Classification by Keeping the Good and Removing the Bad Momentum Causal Effect. In *Proc. of the NeurIPS*, 2020. [10](#)
- [27] Tao Wang, Yu Li, Bingyi Kang, Junnan Li, Jun Hao Liew, Sheng Tang, Steven C. H. Hoi, and Jiashi Feng. The Devil Is in Classification: A Simple Framework for Long-Tail Instance Segmentation. In *Proc. of the ECCV*, pages 728–744, 2020. [10](#)
- [28] Yisen Wang, Difan Zou, Jinfeng Yi, James Bailey, Xingjun Ma, and Quanquan Gu. Improving Adversarial Robustness Requires Revisiting Misclassified Examples. In *Proc. of the ICLR*, 2020. [6](#), [10](#)

- [29] Yu-Xiong Wang, Deva Ramanan, and Martial Hebert. Learning to Model the Tail. In *Proc. of the NeurIPS*, pages 7029–7039, 2017. 1, 4, 7
- [30] Dongxian Wu, Shu-Tao Xia, and Yisen Wang. Adversarial Weight Perturbation Helps Robust Generalization. In *Proc. of the NeurIPS*, 2020. 10
- [31] Tong Wu, Ziwei Liu, Qingqiu Huang, Yu Wang, and Dahua Lin. Adversarial Robustness Under Long-Tailed Distribution. In *Proc. of the CVPR*, pages 8659–8668, 2021. 1, 2, 3, 5, 6, 7, 8, 10
- [32] Tz-Ying Wu, Pedro Morgado, Pei Wang, Chih-Hui Ho, and Nuno Vasconcelos. Solving Long-Tailed Recognition with Deep Realistic Taxonomic Classifier. In *Proc. of the ECCV*, pages 171–189, 2020. 10
- [33] Xi Yin, Xiang Yu, Kihyuk Sohn, Xiaoming Liu, and Manmohan Chandraker. Feature Transfer Learning for Face Recognition With Under-Represented Data. In *Proc. of the CVPR*, pages 5704–5713, 2019. 10
- [34] Sergey Zagoruyko and Nikos Komodakis. Wide Residual Networks. In *Proc. of the BMVC*, 2016. 6
- [35] Hongyang Zhang, Yaodong Yu, Jiantao Jiao, Eric P. Xing, Laurent El Ghaoui, and Michael I. Jordan. Theoretically Principled Trade-off between Robustness and Accuracy. In *Proc. of the ICML*, pages 7472–7482, 2019. 3, 6, 10
- [36] Haizhong Zheng, Ziqi Zhang, Juncheng Gu, Honglak Lee, and Atul Prakash. Efficient adversarial training with transferable adversarial examples. In *Proc. of the CVPR*, pages 1178–1187, 2020. 4

A. Related Works

A.1. Long-tailed Recognition

Long-tailed learning means training a machine learning model on a dataset that follows a long-tailed distribution. It has been applied to various scenarios including classification tasks [24], object detection tasks [19] and segmentation tasks [27]. To alleviate the uneven distribution of data in the dataset, i.e., the majority of the data belong to the head classes, while the data belonging to the tail classes are insufficient, many methods have been proposed, which can be roughly divided into four categories: re-sampling, cost-sensitive learning, training phase decoupling and classifier designing.

The re-sampling methods can be divided into four classes, i.e., random under-sampling head classes [20], random over-sampling tail classes [8], class-balanced re-sampling [24] and scheme-oriented sampling [12]. These methods solve the unbalance problem by using sampling strategies to generate desired balanced distributions.

The cost-sensitive learning methods have two types of applications, i.e., class-level re-weighting [6, 11, 19] and class-level re-margining [3, 17, 31]. It assigns different weights to each class or adjust the minimal margin between the features and the classifier to balance the learning diffi-

culties, achieving better performance under unbalanced data distributions.

The training phase decoupling is used to improve both the feature extractor and classifier. [15] find that training the feature extractor with instance-balanced re-sampling strategy and re-adjusting the classifier can significantly improve the accuracy in long-tailed recognition. [16] further observe that a balanced feature space benefits the long-tailed recognition.

The classifier designing aims to address the biases that the weight norms for head classes are larger than them of tail classes [33] in the traditional layers under long-tailed datasets. [15] propose a normalized classification layer to re-balance the weight norms for all classes. [31] also adopt a normalized classifier to defend against adversarial attacks. [32] propose a hierarchical classifier mapping the images into a class taxonomic tree structure. [26] propose a classifier with causal inference to better stabilize the gradients. Note that modifying the classifier can indeed improve the performance of models on unbalanced data. However, we argue that it may introduce gradient obfuscation resulting in adaptive adversarial attacks. For more details, please refer to Section 5 in the main paper.

A.2. Adversarial Training

Adversarial training [21, 25, 28, 35] is widely studied to defend against adversarial attacks. Its basic idea is to generate on-the-fly AEs to augment the training set. It can be formulated as the following min-max problem [21]:

$$\min_{\theta} \max_{x^*} \ell(x^*, y; \theta)$$

where x^* is the training sample generated from a clean one x to maximize the loss function $\ell(\cdot)$, y is the ground-truth label, θ is the model parameters. The first phase (maximization optimization) is to generate samples maximizing the loss function. The second stage (minimization optimization) is to optimize the model parameter θ to minimize the loss function under samples generated in phase one.

In previous works, there are three main research topics in adversarial training, i.e., improving the model robustness [21, 28], reducing the gap between clean accuracy and robustness [30, 35] and addressing overfitting challenges [13, 25].

In this paper, we focus on adversarial training on datasets with long-tailed distributions. To our best knowledge, [31] present the first work dedicated to improving the accuracy as well as robustness to tail class during adversarial training. They design a new loss function and cosine classifier to achieve this. However, we experimentally demonstrate the unsatisfactory security and performance of this work in Section 5.2, which motivates us to design more secure and satisfactory adversarial training methods tailored to datasets that obey long-tailed distributions.

B. Proof

Theorem 2 Given a function f_θ and dataset \mathcal{D} , which we defined above, let

$$g(x) \in \operatorname{argmax}_{x' \in \mathcal{B}_p(x, \epsilon)} \mathbb{1}\{F_\theta(x) \neq F_\theta(x')\}$$

Assume that a larger n_i will decrease the $\mathcal{R}_{\text{rob}}^i(\theta)$, and vice versa. Then, we have

$$\begin{aligned} \mathcal{R}_{\text{rob}}(\theta) &\geq \sum_{i=1}^C \frac{1}{C} \left(\sum_{j=1}^{n_i} \mathbb{1}\{F_\theta(x_i^j) \neq i\} \right. \\ &\quad \left. + \sum_{j=1}^{n_i} \mathbb{1}\{F_\theta(g(x_i^j)) \neq F_\theta(x_i^j)\} \right) \end{aligned}$$

Proof 1 We have

$$\begin{aligned} \mathcal{R}_{\text{bdy}}^i(\theta) &= \sum_{j=1}^{n_i} \mathbb{1}\{\exists x' \in \mathcal{B}_p(x_i^j, \epsilon), F_\theta(x') \neq i\} p(i) \\ &\geq \sum_{j=1}^{n_i} (\mathbb{1}\{F_\theta(g(x_i^j)) \neq F_\theta(x_i^j), F_\theta(x_i^j) = i\} \\ &\quad + \mathbb{1}\{F_\theta(g(x_i^j)) \neq F_\theta(x_i^j), F_\theta(x_i^j) \neq i\}) p(i) \\ &= \sum_{j=1}^{n_i} (\mathbb{1}\{F_\theta(g(x_i^j)) \neq F_\theta(x_i^j)\} \mathbb{1}\{F_\theta(x_i^j) = i\} \\ &\quad + \mathbb{1}\{F_\theta(g(x_i^j)) \neq F_\theta(x_i^j)\} \mathbb{1}\{F_\theta(x_i^j) \neq i\}) p(i) \end{aligned}$$

Let $\mathcal{A} = \mathbb{1}\{F_\theta(x_i^j) \neq i\}$ and $\mathcal{B} = \mathbb{1}\{F_\theta(g(x_i^j)) \neq F_\theta(x_i^j)\}$, we have

$$\begin{aligned} \mathcal{R}_{\text{rob}}(\theta) &\geq \sum_{i=1}^C p(i) \left(\sum_{j=1}^{n_i} \mathcal{A} + \mathcal{B}(1 - \mathcal{A}) + \mathcal{B}\mathcal{A} \right) \\ &= \sum_{i=1}^C p(i) \left(\sum_{j=1}^{n_i} \mathcal{A} + \mathcal{B} \right) \end{aligned}$$

Based on the assumption and Chebyshev inequality, we have

$$\begin{aligned} \mathcal{R}_{\text{rob}}(\theta) &\geq \sum_{i=1}^C \frac{1}{C} \left(\sum_{j=1}^{n_i} \mathcal{A} + \mathcal{B} \right) \\ &= \sum_{i=1}^C \frac{1}{C} \left(\sum_{j=1}^{n_i} \mathbb{1}\{F_\theta(x_i^j) \neq i\} \right. \\ &\quad \left. + \sum_{j=1}^{n_i} \mathbb{1}\{F_\theta(g(x_i^j)) \neq F_\theta(x_i^j)\} \right) \end{aligned}$$

C. Evaluation on Real-World Dataset

We consider a real-world dataset, Tiny-Imagenet, to evaluate our method. Because RoBal does not provide the hyperparameters for this dataset, we compare REAT with PGD-AT

method. We randomly downsample the training set, to obtain a long-tailed subset. In detail, the number of data in each class decreases linearly. In our subset, the UR is 100, which means the class with the most data contains 500 images, and the class with the fewest data contains 5 images. We train a ResNet-18 on this subset with PGD-AT and REAT, respectively. The results can be found in Table 6. From the results, we can find that our method performs better than the baseline method with about 2% 3% improvement on clean accuracy and robust accuracy. Therefore, our approach is a better choice for solving real-world long-tail challenges.

Model	Clean Accuracy	PGD-20	PGD-100	CW-100	AA
PGD-AT	40.29	30.66	30.65	29.10	28.73
REAT	43.09	33.00	33.00	31.16	30.74

Table 6. Evaluation on the real-world dataset, Tiny-Imagenet. The attack budget is $\epsilon = 2/255$.

D. Adversarial Training on Unbalanced Dataset

To explore the effectiveness of adversarial training strategies proposed on balanced datasets, we compare recent adversarial training methods in Table 7. The results indicate that improving robustness on a balanced dataset is non-trivial, but these improvements cannot be expressed under an unbalanced dataset. Furthermore, we find that the simplest and the most straightforward method, PGD-AT, obtains the best results. On the other hand, methods adopting clean samples to train models, like TRADES and MART, will achieve lower clean accuracy, as the unbalanced data will harm the model’s accuracy on the balanced test set.

In Figure 7, the t-SNE results prove that each class is assigned an area of a similar size in the feature space when the model is trained on balanced data. But, if the model is trained on unbalanced data, the areas for head classes expand and encroach areas that should belong to tail classes, causing the area of tail features to shrink, which represents the **unbalanced feature embedding space**. As a result, the performance and generalizability for tail classes decrease.

To alleviate the unbalance problem, we replace the cross-entropy loss in TRADES and MART with Balanced Softmax Loss (BSL). However, in our experiments, we find that BSL will make the model not converge. The reason can be that the gradient directions of BSL and KL divergence are contradicted. So, in our paper, we mainly consider enhancing the PGD-AT method to better fit the unbalanced datasets.

E. Studying Data Hunger and Data Unbalance

In this part, we further examine the effects of the data hunger and the data unbalance on the model robustness, which is explored to construct an experimental upper bound on the robustness of the long-tailed adversarial training methods. To be specific, the data hunger raises from the insufficient

Method	Clean Accuracy	PGD-20	PGD-100	CW-100	AA
PGD-AT	51.28(1.34)	29.57(0.17)	29.47(0.15)	29.05(0.07)	27.71(0.15)
TRADES	45.55(0.89)	28.24(0.21)	28.21(0.20)	27.29(0.17)	26.78(0.10)
PGD-AWP	36.45(3.40)	26.52(1.64)	26.47(1.62)	26.04(1.54)	25.23(1.47)
TRADES-AWP	41.30(0.47)	27.04(0.08)	27.00(0.07)	25.65(0.08)	25.37(0.07)
MART	41.76(0.63)	29.18(0.12)	29.14(0.13)	27.04(0.06)	26.06(0.03)

Table 7. Results on CIFAR-10-LT (UR=50) with different training strategies.

UR	Method	Clean Accuracy	PGD-20	PGD-100	CW-100	AA
10	PGD-AT (BS)	77.12(0.73)	44.73(0.20)	44.49(0.20)	43.81(0.26)	41.50(0.19)
	PGD-AT	75.27(0.32)	42.66(0.20)	42.36(0.20)	41.18(0.21)	38.81(0.10)
	REAT	75.20(0.03)	42.97(0.17)	42.76(0.19)	41.52(0.22)	39.25(0.21)
20	PGD-AT (BS)	75.61(0.10)	43.37(0.15)	43.22(0.17)	42.12(0.12)	40.01(0.03)
	PGD-AT	72.31(0.24)	39.79(0.31)	39.61(0.30)	38.42(0.06)	36.18(0.03)
	REAT	72.73(0.50)	40.57(0.15)	40.41(0.12)	38.55(0.29)	36.53(0.21)
50	PGD-AT (BS)	72.98(0.74)	41.14(0.26)	40.89(0.30)	39.92(0.49)	37.75(0.40)
	PGD-AT	66.99(0.17)	35.23(0.45)	35.01(0.43)	33.17(0.37)	31.15(0.49)
	REAT	67.33(0.45)	36.20(0.06)	36.02(0.09)	33.98(0.23)	32.08(0.12)
100	PGD-AT (BS)	72.83(0.53)	40.25(0.35)	40.10(0.45)	39.29(0.19)	37.24(0.18)
	PGD-AT	62.70(0.52)	32.91(0.17)	32.73(0.19)	30.45(0.15)	28.60(0.21)
	REAT	63.92(0.68)	32.84(0.07)	32.69(0.15)	30.73(0.38)	28.90(0.33)

Table 8. Results on CIFAR-10 and CIFAR-10-LT with different URs. BSL loss is adopted for PGD-AT and REAT.

data from the body classes and tail classes, which is one of the impacts of the long-tailed datasets. And another one is the data unbalance. To exclusively study the data hunger in a balanced dataset, for a given unbalanced ratio, we sample the same number of samples as the long-tail dataset but form them into balanced small (BS) datasets. We then train models on this dataset with PGD-AT to learn an experimental upper bound, which is represented as “PGD-AT (BS)” in our experiments. When we train models with PGD-AT (BS) the loss function used to optimize models is Cross-Entropy loss.

On the other hand, when we train models on unbalanced datasets, the basic loss function used to optimize models is BSL.

Comparing the results of models trained under balanced datasets and unbalanced datasets in Tables 8–11, it is clear that the models train on unbalanced datasets suffer from a bigger reduction when the number of training samples decreases, which means that the data unbalance harms the model’s robustness in a larger degree than the data hunger. Training models on unbalanced data is more challenging

UR	Method	Clean Accuracy	PGD-20	PGD-100	CW-100	AA
10	PGD-AT (BS)	48.32(0.50)	20.08(0.24)	19.95(0.25)	18.88(0.28)	17.44(0.21)
	PGD-AT	45.96(0.49)	18.85(0.19)	18.73(0.17)	17.70(0.13)	16.21(0.13)
	REAT	45.94(0.15)	19.26(0.18)	19.16(0.18)	17.99(0.09)	16.58(0.06)
20	PGD-AT (BS)	45.14(0.28)	17.95(0.19)	17.82(0.17)	17.15(0.19)	15.80(0.23)
	PGD-AT	42.45(0.53)	16.36(0.13)	16.24(0.14)	15.47(0.17)	14.17(0.09)
	REAT	41.98(0.21)	16.84(0.10)	16.72(0.12)	15.77(0.23)	14.45(0.20)
50	PGD-AT (BS)	42.86(0.37)	16.52(0.26)	16.38(0.24)	15.86(0.14)	14.54(0.05)
	PGD-AT	37.70(0.12)	13.95(0.07)	13.86(0.05)	13.17(0.11)	12.10(0.02)
	REAT	37.43(0.37)	14.25(0.22)	14.18(0.26)	13.38(0.15)	12.32(0.17)

Table 9. Results on CIFAR-100 and CIFAR-100-LT with different URs. BSL loss is adopted for PGD-AT and REAT.

Method		Clean Accuracy	PGD-20	PGD-100	CW-100	AA
ResNet	PGD-AT (BS)	72.98(0.74)	41.14(0.26)	40.89(0.30)	39.92(0.49)	37.75(0.40)
	PGD-AT	66.99(0.17)	35.23(0.45)	35.01(0.43)	33.17(0.37)	31.15(0.49)
	REAT	67.33(0.45)	36.20(0.06)	36.02(0.09)	33.98(0.23)	32.08(0.12)
WRN	PGD-AT (BS)	78.65(0.15)	42.42(0.33)	42.05(0.32)	42.21(0.08)	39.86(0.37)
	PGD-AT	72.38(0.30)	35.93(0.10)	35.64(0.04)	34.93(0.14)	32.84(0.19)
	REAT	72.58(0.31)	36.53(0.31)	36.35(0.32)	35.30(0.37)	33.37(0.37)

Table 10. Results on CIFAR-10 and CIFAR-10-LT (UR=50) with different model structures. BSL loss is adopted for PGD-AT and REAT.

Method		Clean Accuracy	PGD-20	PGD-100	CW-100	AA
ResNet	PGD-AT (BS)	48.32(0.50)	20.08(0.24)	19.95(0.25)	18.88(0.28)	17.44(0.21)
	PGD-AT	45.96(0.49)	18.85(0.19)	18.73(0.17)	17.70(0.13)	16.21(0.13)
	REAT	45.94(0.15)	19.26(0.18)	19.16(0.18)	17.99(0.09)	16.58(0.06)
WRN	PGD-AT (BS)	52.33(0.42)	21.95(0.10)	21.77(0.14)	21.41(0.20)	19.58(0.17)
	PGD-AT	50.07(0.25)	20.79(0.39)	20.69(0.38)	20.17(0.27)	18.32(0.28)
	REAT	49.99(0.18)	20.85(0.16)	20.71(0.20)	20.18(0.09)	18.35(0.17)

Table 11. Results on CIFAR-100 and CIFAR-100-LT (UR=10) with different model structures. BSL loss is adopted for PGD-AT and REAT.

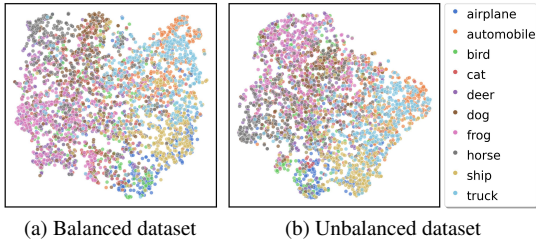


Figure 7. AE’s feature t-SNE results for ResNet-18 trained with PGD-AT on balanced and unbalanced CIFAR-10.

than training models on small but balanced data under adversarial scenarios for different model structures and datasets. It is reasonable, because in the long-tailed datasets, there are fewer data in the tail classes, making the model unable to learn much information for such classes. Furthermore, compared with training a model on CIFAR-10, when training a model on a more complex dataset, such as CIFAR-100, the performance decrease is less than expected, which will be studied in our future work. On the other hand, the experimental results of PGD-AT (BS) can be seen as upper bounds for the models trained on same-size unbalanced datasets.

F. Results under l_2 -norm Attacks

In Table 12, we show the results of models under l_2 -norm attacks. For the PGD attacks, the max perturbation size is $\epsilon = 1.0$, and the step length is $\alpha = 0.2$. We consider the 20-step attack, PGD-20, and the 100-step attack, PGD-100. For the C&W attack, we follow its official implementation. The results confirm that our REAT can improve the model’s

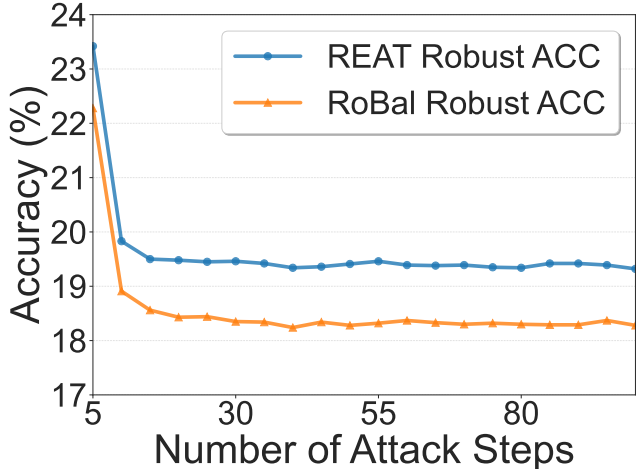


Figure 8. Accuracy of Attack Steps on CIFAR-100-LT (UR=10). robustness under different threat models. On the other hand, the gradient obfuscation is more serious under l_2 -norm attacks, so our adaptive attacks achieve better results.

G. Comparing with RoBal

Varying Datasets. Similar to our main paper, we illustrate the robust accuracy under the different numbers of PGD attack steps of ResNet-18 on CIFAR-100-LT (UR=10) in Figure 8 in this section. The results prove that our REAT outperforms RoBal under all attack budgets. In Figure 9, we plot the accuracy of ResNet-18 on CIFAR-100-LT (UR=10) under the PGD-20 attack for each class. The results indicate that our REAT can achieve higher clean accuracy and robust accuracy on “body” classes, which is consistent with the

UR	Method	Clean Accuracy	PGD-20	PGD-100	CW
10	PGD-AT	75.27(0.32)	30.92(0.47)	28.82(0.63)	70.76(0.20)
	RoBal	75.33(0.39)	33.15/ 28.26 (0.62)	31.43/ 26.18 (0.80)	71.36(0.39)
	REAT	75.20(0.03)	30.82(0.60)	28.71(0.74)	71.02(0.18)
20	PGD-AT	72.31(0.24)	29.23(0.50)	27.24(0.55)	67.87(0.26)
	RoBal	71.92(0.62)	31.79/ 27.13 (0.37)	30.34/ 25.38 (0.44)	67.95(0.58)
	REAT	72.73(0.50)	29.27(0.58)	27.44(0.59)	68.13(0.43)
50	PGD-AT	66.99(0.17)	26.75(0.31)	25.20(0.31)	62.54(0.14)
	RoBal	66.08(0.69)	29.22/ 24.17 (0.68)	27.97/ 22.83 (0.60)	62.03(0.65)
	REAT	67.33(0.45)	27.45(0.30)	25.91(0.40)	63.08(0.23)
100	PGD-AT	62.70(0.52)	24.91(0.46)	23.49(0.42)	58.06(0.40)
	RoBal	60.11(0.62)	27.77/ 23.33 (0.46)	26.48/ 21.91 (0.43)	56.34(0.28)
	REAT	63.92(0.68)	24.63(0.21)	23.24(0.21)	59.17(0.49)

Table 12. Results on CIFAR-10-LT with different URs under l_2 -norm attacks. Red numbers represent the results under our adaptive attack. BSL loss is adopted for PGD-AT and REAT.

Method		Clean Accuracy	PGD-20	PGD-100	CW-100	AA
ResNet	RoBal	43.47(0.31)	20.55(0.20)	20.49(0.20)	18.12(0.23)	16.86(0.10)
	REAT	45.94(0.15)	19.26(0.18)	19.16(0.18)	17.99(0.09)	16.58(0.06)
WRN	RoBal	48.84(0.24)	21.45(0.18)	21.44(0.21)	19.71(0.09)	18.21(0.02)
	REAT	49.99(0.18)	20.85(0.16)	20.71(0.20)	20.18(0.09)	18.35(0.17)

Table 13. Results on CIFAR-100-LT (UR=10) with different model structures. Red numbers represent the results under our adaptive attack. BSL loss is adopted for REAT.

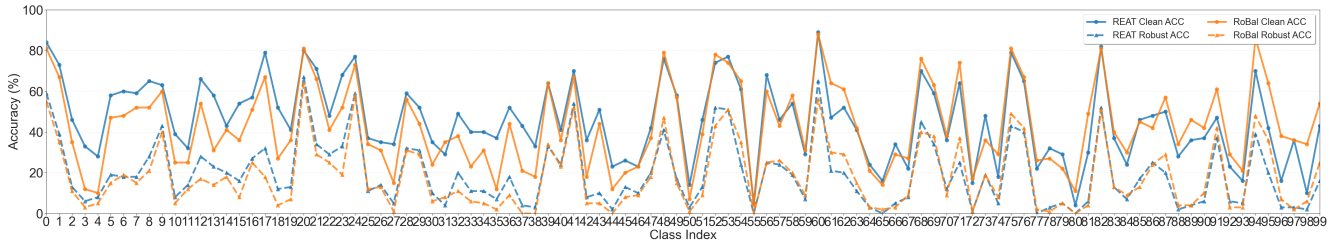


Figure 9. Accuracy of Each Class on CIFAR-100-LT (UR=10).

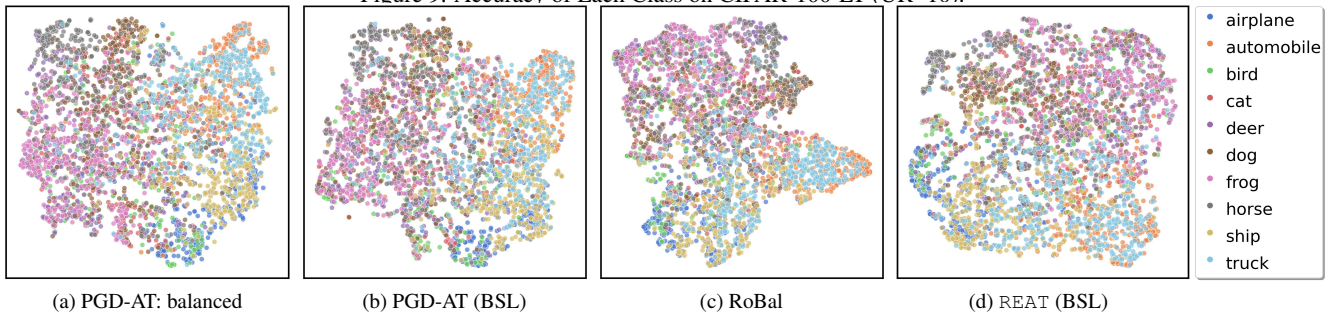


Figure 10. AE's feature map results with different strategies. (a) is trained with the balanced dataset (CIFAR-10) while the rest three are trained with the unbalanced dataset (CIFAR-10-LT, UR=50).

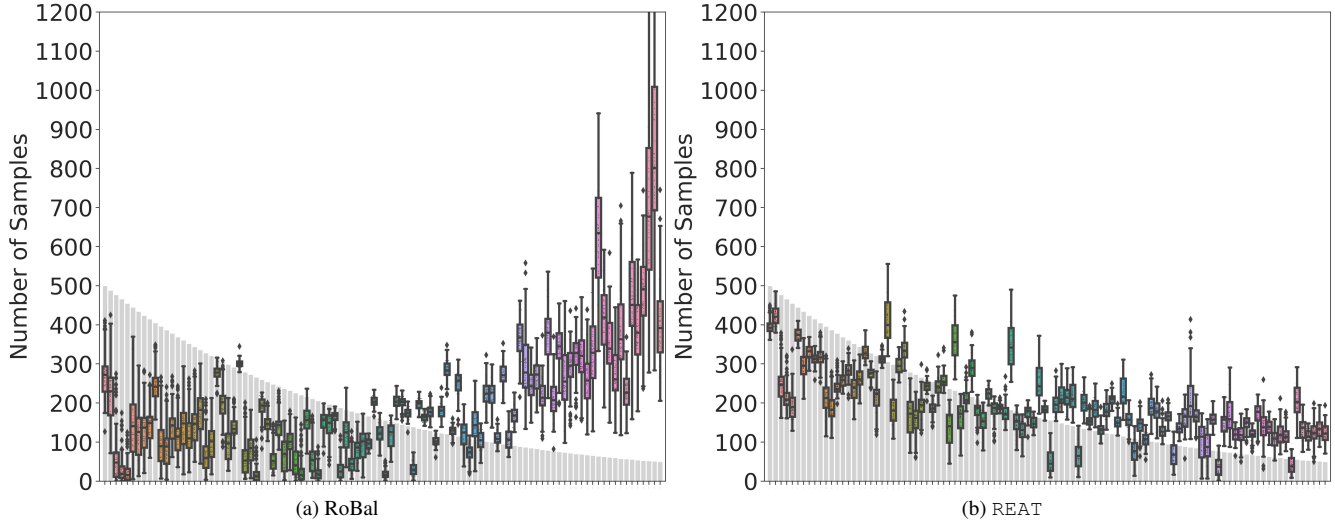


Figure 11. The distribution of model predictions for AEs during the training process on CIFAR-100-LT (UR=10). Clean label distributions are shown by gray bars.

conclusion in the main paper.

Varying Model Structures. To show the superiority of REAT on different model structures, we compare the results of RoBal and REAT on ResNet-18 and WideResNet-28-10, respectively. The results in Table 13 prove that models trained with REAT lead models trained with RoBal on both clean accuracy and robustness, which means REAT is a better training strategy for different model structures.

Interpretation. We choose the configurations of CIFAR-10-LT (UR=50) and ResNet-18. Then, we plot the feature embedding space with the t-SNE tool for models trained with different strategies in Figure 10. We first generate AEs with the PGD-20 attack on the test set and use t-SNE to plot the feature distribution for AEs. ResNet-18 is adopted as the model architecture. Figure 10a is the feature result for PGD-AT over the balanced dataset CIFAR-10. We observe that samples from different classes are not quite overlapped with each other in the feature space, making them easier to be classified. In contrast, Figures 10b and 10c show the results for PGD-AT (BSL loss) and RoBal over the unbalanced dataset CIFAR-10. We observe that there are more samples from different classes entangled together in their feature embeddings, which can harm the model’s robustness. Figure 10d shows the results of our REAT under the same unbalanced setting. We can see the feature space is more similar to the one obtained from the balanced dataset (Figure 10a). This explains the effectiveness of REAT in enhancing the model robustness and clean accuracy from the feature perspective.

H. AE Prediction Distribution

In Figure 11, we compare the AE distribution on CIFAR-100-LT (UR=10), when training models with RoBal and

REAT, respectively. The results prove that RoBal will cause unbalanced AE distribution when the number of classes increases. There are more samples predicted as tail classes by the model. However, our REAT can keep the balanced AE distribution and obtain better results.

I. Training Cost Overhead of REAT

We compare the training time overhead of REAT compared with PGD-AT (BSL is adopted) method and RoBal on one single V100 GPU card. The results are shown in Table 14. When we train a ResNet-18 on CIFAR-10-LT (UR=50), the training time overhead for one epoch is about 8 seconds. When we train a ResNet-18 on CIFAR-10-LT (UR=100), the training time overhead for one epoch is about 5 seconds. So, our REAT is efficient on long-tailed datasets and does not increase too much training time.

Dataset	UR	Time Cost (Secs)		
		PGD-AT	RoBal	REAT
CIFAR-10-LT	50	46	50	54
	100	42	45	47
CIFAR-100-LT	20	53	58	75
	50	42	45	52

Table 14. Time cost (seconds) for one training epoch on CIFAR-10-LT and CIFAR-100-LT. The model is ResNet-18. BSL loss is adopted for PGD-AT and REAT.